Lecture Notes in Applied and Computational Mechanics 93

Peter Wriggers
Olivier Allix
Christian Weißenfels *Editors*

Virtual Design and Validation

Springer

Lecture Notes in Applied and Computational Mechanics

Volume 93

This series aims to report new developments in applied and computational mechanics—quickly, informally and at a high level. This includes the fields of fluid, solid and structural mechanics, dynamics and control, and related disciplines. The applied methods can be of analytical, numerical and computational nature. The series scope includes monographs, professional books, selected contributions from specialized conferences or workshops, edited volumes, as well as outstanding advanced textbooks.

Indexed by EI-Compendex, SCOPUS, Zentralblatt Math, Ulrich's, Current Mathematical Publications, Mathematical Reviews and MetaPress.

More information about this series at http://www.springer.com/series/4623

Peter Wriggers · Olivier Allix ·
Christian Weißenfels
Editors

Virtual Design and Validation

Springer

Editors
Peter Wriggers
Institut für Kontinuumsmechanik
Leibniz Universität Hannover
Hannover, Germany

Olivier Allix
LMT-Cachan
Cachan, France

Christian Weißenfels
Institut für Kontinuumsmechanik
Leibniz Universität Hannover
Hannover, Germany

ISSN 1613-7736 ISSN 1860-0816 (electronic)
Lecture Notes in Applied and Computational Mechanics
ISBN 978-3-030-38155-4 ISBN 978-3-030-38156-1 (eBook)
https://doi.org/10.1007/978-3-030-38156-1

This Springer imprint is published by the registered company Springer Nature Switzerland AG
The registered company address is: Gewerbestrasse 11, 6330 Cham, Switzerland

Preface

Particularly in the aerospace and automotive industries, the need for weight-optimized structures is growing to ensure low-consumption operations. Simultaneously, the load-bearing capacity and safety requirements must be guaranteed. This requires new materials and innovative structures. The vision in engineering is a purely virtual development of new materials, components and assemblies on the computer. Compared to an experimentally based development, simulation driven engineering enables an acceleration of the development process while reducing costs. Different scenarios can be checked using virtual computer simulations until the optimal material or structure is found. Changes on the micro- or nanoscale enable the virtual creation of new materials. The behavior of these materials can be tested directly on the computer under real conditions. Simulations can also be used to predict changes in the materials over a longer period of time. For the structural change towards a purely digital development process in industry, mathematical models are needed, which describe the behavior of materials and structures under loading realistically, as well as suitable algorithms and solution methods, which solve these equations accurately and efficiently.

This book contains 17 articles that have emerged from selected works of the International Research Group IRTG 1627. A special focus of the German–French cooperation is the experimental characterization of materials and their numerical modeling, as well as the development of new computational methods for a virtual design.

The selected contributions are assigned to four thematic areas: Experiments and virtual design, composites, fracture and fatigue and uncertainty quantification.

The first area relates to new experimental methods that can be used to characterize material behavior more accurately. Furthermore, a combined experimental and numerical approach is presented to optimize the properties of a structure. Besides the modeling of MEMS, new developments in the field of computational methods for virtual design are presented.

The second topic is dedicated to experimental and numerical investigations of composites. A special focus is on the modeling of failure modes and the optimization of these materials.

New numerical schemes in the field of crack modeling and fatigue prediction are discussed in the third area. Fatigue also includes wear due to frictional contact and ageing of elastomers.

The input parameters of a numerical simulation classically represent mean values of real observations. However, more or less strong deviations occur. To illustrate the uncertainties of parameters in calculations, new and efficient approaches are presented in the last section.

All contributions provide a good overview of the state-of-the-art approaches and future developments in the field of virtual design.

Hannover, Germany — Peter Wriggers
Cachan, France — Olivier Allix
Hannover, Germany — Christian Weißenfels

Contents

Experiments and Virtual Design

Digital Volume Correlation of Laminographic and Tomographic Images: Results and Challenges

Amine Bouterf, Ante Buljac, François Hild, Clément Jailin, Jan Neggers and Stéphane Roux

Abstract Although digital volume correlation (DVC) seems to be a simple extension of digital image correlation to 3D situations, new challenges arise. The first problem is that the actual microstructure of the material can hardly be varied overall to improve the contrast. The applicability of the technique may therefore seem limited to a restricted class of materials. Artifacts during image acquisition and/or reconstruction potentially have a more dramatic effect than noise on the calculated displacement field. Because the acquisition time is generally long, the time sampling is very low compared to the spatial sampling. Moreover, experiments have to be interrupted during acquisition to "freeze" out motions, thereby making time-dependent behavior out of reach. Handling large amounts of data is another challenge. To cope with these complications, specific developments must be designed, the most important of which are mechanics-based regularizations that constrain the desired field of motion to compensate for the adverse effects of noise, artifacts and/or poor texture. With such strategies, DVC offers an unprecedented wealth of information to analyze the mechanical behavior of a large class of materials.

1 Introduction

Digital volume correlation (DVC) allows for the measurement of displacement fields from 3D images acquired for example with X-ray tomography (X-CT) systems [1]. Similarly, imaging thin plates (as opposed to stick-like samples in tomography) is possible via synchrotron laminography [2]. DVC is a direct extension of digital image correlation (DIC), and therefore different strategies developed in 2D were generalized to 3D with similar weaknesses or advantages [3, 4].

A. Bouterf · A. Buljac · F. Hild (✉) · C. Jailin · J. Neggers · S. Roux
Université Paris-Saclay, ENS Paris-Saclay, CNRS, Laboratoire de mécanique et technologie, 61 avenue du Président Wilson, 94235 Cachan Cedex, France
e-mail: francois.hild@ens-paris-saclay.fr

P. Wriggers et al. (eds.), *Virtual Design and Validation*, Lecture Notes in Applied and Computational Mechanics 93, https://doi.org/10.1007/978-3-030-38156-1_1

In the same way that DIC is gradually being routinely used in solid mechanics, it is likely that DVC will experience a similar development over the next decade, as tomographs will become more and more common instruments [1, 5]. The invaluable information provided by tomography in the field of materials science has been mainly focused on 3D imaging of various microstructures. Using 3D image analysis techniques, the access to constitutive phases of a material, their morphology, the statistical characterization of the number, size and shape of inclusions, pores, grains has been the subject of much attention, and this effort has been very rewarding [6–8]. A second very attractive potential of computed tomography in the industrial context is the shape metrology [9]. This application pushed tomography to become even more quantitative than what was asked in simple imaging. This being also achieved for laboratory tomographs, it is now very tempting to follow the deformation of a specimen during mechanical loading, so that in situ mechanical tests constitute an expanding field of investigation [10]. In all these areas, DVC is the preferred technique for measuring three-dimensional displacement fields and coupling experiments with modeling [11–13].

This chapter highlights the new challenges specifically related to DVC and the recently implemented developments to address these demands.

2 Challenges

2.1 Material Microstructure

The first generic difficulty is that the actual microstructure of the material can hardly be modified in bulk in order to improve its X-ray absorption contrast. Some attempts have been made (e.g., adding particles [14] or revealing the boundaries of grains [15]), but at the risk that the material has a different behavior than with no contrast enhancement. This is a major difference from 2D-DIC, in which a homogeneous or transparent material can always be painted with a speckle pattern, where the experimenter can adjust the homogeneity, correlation length of the pattern and contrast more or less at will [3]. In synchrotron facilities, the use of phase contrast can reinforce the differences between the material phases and make them visible on radiographs [16–18].

Such severe conditions push DVC to deal with microstructures that can be very faint, with very few contrasting phases, possibly with a low contrast compared to reconstruction artifacts (Fig. 1c). Robustness when confronted to such sparse contrast is a major challenge that limits a priori the use of DVC to specific microstructures (e.g., biological tissues [19], foams [20] and cellular materials (Fig. 1a), or materials with a large proportion of inclusions [11, 21, 22], see Fig. 1b).

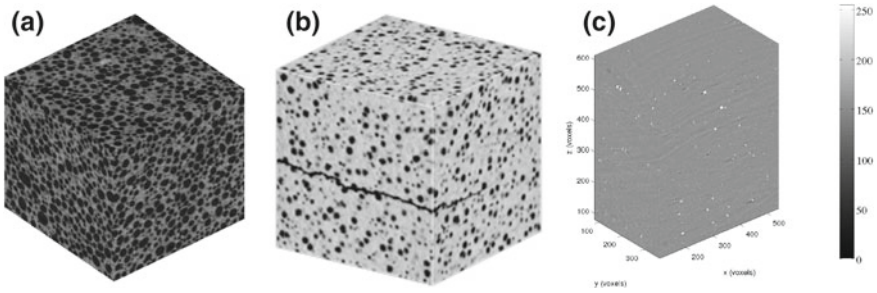

Fig. 1 3D rendering of three different textures. **a** Plaster with a volume fraction of void of 56% (1 voxel ↔ 48 µm). **b** Spheroidal graphite cast iron with a 13% volume fraction of graphite nodules (1 voxel ↔ 5.1 µm). **c** Aluminum alloy with 0.3–0.4% of secondary particles (1 voxel ↔ 0.7 µm)

2.2 CT Imaging and Artifacts

Tomographic imaging itself poses new challenges, namely that artifacts when acquiring or reconstructing images can affect the calculated displacement field. For example, in a laboratory tomographic scanner, a minute shift of the source may cause a change in magnification of the image, and therefore a uniform apparent expansion not to be confused with mechanical strains [23]. For this reason, many recent laboratory systems have thermal regulation that limits this bias. Yet, an experiment lasting several days remains quite difficult.

Further, a defective pixel on the detector, a bad "flat field" normalization or more generally any deviation from the general assumptions (such as the displacement occurring during the scan) usually induces "ring artifacts" [24]. The presence of reconstruction artifacts (such as rings) becomes very detrimental when the contrast due to the natural microstructure of the material is low. It is therefore very important to treat these cases in order to make DVC useful for a wider class of materials. In addition to the progress of the reconstruction technique itself, one solution to the problem is to digitally filter the images before DVC analyses are run (e.g., ring artifacts can be significantly reduced [25]). This filtering can however also affect the true microstructure. Another challenge lies in the fact that the actual (reliable) microstructure after filtering may consist of a very faint texture (i.e., low gradients of gray level or very dilute support, see Fig. 1c). To solve this problem while preserving an acceptable spatial resolution, appropriate regularization strategies are needed (Sects. 3.3 and 3.4).

2.3 Volume of Data/Duration of Acquisition

Another limitation comes from the huge amount of information contained in 3D images. This challenge is first met at the acquisition stage, where a complete analysis

may take up to an hour or more in some cases, of such a duration that creep may be responsible for a significant motion between the first and the last radiographs. This bias makes it difficult (if not impossible) for proper standard reconstructions [26]. This limitation can be partly overcome in third generation synchrotron facilities since very energetic beams allow for very short acquisition times (e.g., 45 s [27] and 4 s [28] in the case of thermomechanical tests). When high-speed cameras were utilized, full scans could be performed at 20 Hz frequency. When standard reconstruction algorithms are used, the quality of the reconstructed volumes degrades in comparison to slower acquisitions since they do not account for minute motions induced by the vibrations of the rotation stage [29]. These observations call for combining reconstruction procedures accounting for motions during acquisitions [26].

Second, at the reconstruction stage, the cost of data processing favors fast techniques (such as the well-known Filtered Back-Projection algorithm [30]) rather than algebraic variants, which are more reliable [31], but more demanding in terms of reconstruction. DVC itself also involves a large amount of data and efficient data processing becomes essential. When regularized or integrated strategies are considered (see below), this demand becomes even more severe. Effective GPU implementations can be a solution [32]. However, other strategies may be envisaged, which will require a very significant reduction in the number of radiographs [33]. This last option is extremely appealing because it allows for much faster data acquisitions without having to spin the sample too fast. However, this approach complements missing projection data with a priori information, and its compatibility with DVC registration, where subvoxel resolution is aimed for, remains to be validated.

2.4 Detecting Features Invisible to the Eye

Another difficulty is that some interesting features of the mechanical analysis may not be visible because of insufficient spatial resolution or because some parts of the texture (e.g., particles useful for DVC) exhibit the same gray levels as the desired feature Fig. 1b). An example of this category is the crack opening that cannot be detected when its level is not comparable to the size of the voxel (Fig. 2b). The ability of DVC to detect motions much smaller than the size of the voxel (i.e., of the order of 10^{-1} voxel) is an advantage that was used to evaluate stress intensity factors (see Sect. 3.2). In addition, new techniques were specifically designed for analyzing crack openings and for locating the position of the crack front in 3D long before it could be seen on a single image [11].

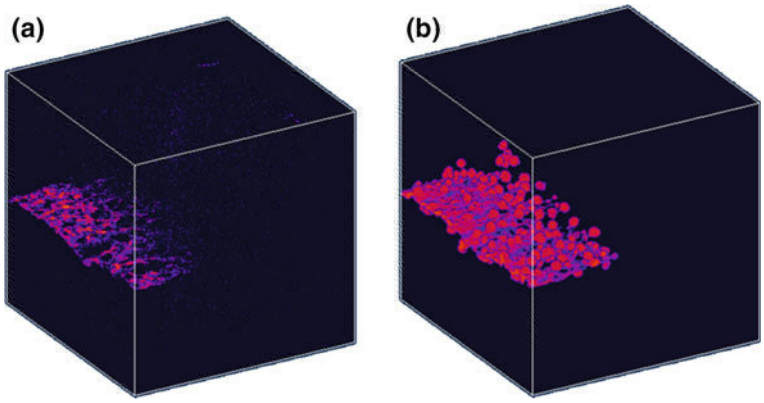

Fig. 2 **a** 3D rendering of correlation residuals clearly locating the crack surface. **b** Thresholded gray levels in the vicinity of the crack surface. It is impossible to locate the crack surface because the nodules and the crack have similar gray levels (Fig. 1b)

3 Recent Solutions

3.1 Filtering 3D Images

The 3D images are reconstructed from radiographs acquired according to different orientations of the sample with respect to the beam so that artifacts may arise. This is especially true when the reconstruction method is known to be approximate [e.g., far from the median plane with fan-beam or cone-beam tomography or in laminography (Fig. 3)]. Moreover, phase contrast between the particles and the matrix leads to a spurious "aura" around each particle that fades away with distance. This pattern is fake, but it moves together with the particle (yet it does not rotate with it). Hence it helps DVC but can only be trusted if local rotations are not sought.

Filtering of reconstructed images to erase the ring artifacts while preserving the microstructure can be performed as illustrated in Fig. 3b. As a result, it is found that the gray level histogram, which was already rather poor for DVC purposes, becomes even narrower (Fig. 4). Assuming that this thinning of the histogram is mainly due to the correction of artifacts, it shows that the recourse to the texture of the direct reconstructions may lead to false evaluations of the displacements, because the rings do not necessarily follow the kinematics of the material. For this particular case, the initial amount of inclusions in the material was estimated to be about 0.3–0.4 vol%. It should be noted that a direct attempt to use DVC on filtered images does not lead to convergence. Such a poor microstructural texture makes the ill-posed nature of DVC more difficult. In a forthcoming section, it will be shown that DVC can be used on unfiltered images, because in this particular case, the artifacts come from phase contrast, and are therefore advected with the inclusions. Note, however, that the rings do not rotate with the microstructure of the material and are therefore fragile markers for DVC purposes.

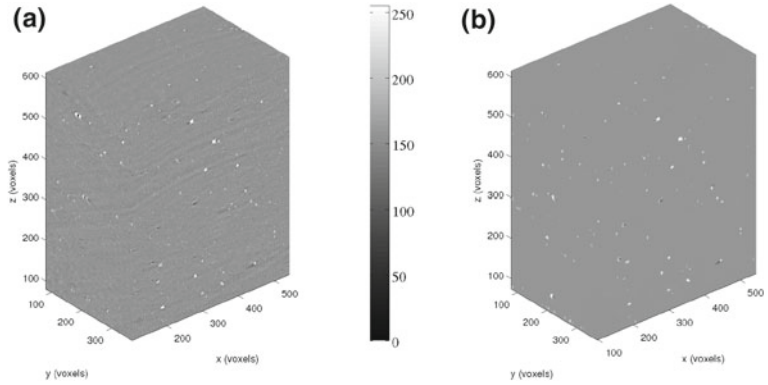

Fig. 3 3D rendering of an aluminum alloy with 0.3–0.4 vol% of secondary particles (1 voxel ↔ 0.7 µm). **a** Raw reconstructed volume, and **b** filtered reconstruction

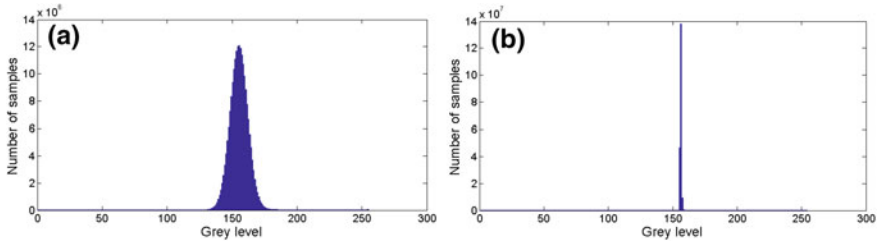

Fig. 4 Gray level histograms of aluminum alloy laminographies (Fig. 3). **a** Raw reconstructed volume, and **b** filtered reconstruction

3.2 Global DVC

Parallel to the distinction between local and global DIC strategies [34, 35], the two propositions can simply be extended to DVC. In fact, from a theoretical point of view, spatial dimensionality does not play a key role in image registration. Local DVC consists in analyzing sub-volumes and determining their average displacements from the recording of a deformed sub-volume corrected with the corresponding reference [19, 36]. These corrections may involve a linear displacement gradient, although only the average displacement is retained.

Global DVC consists in seeking the "best" displacement field in a specified kinematic vector space defined over the whole region of interest. A common choice of this space is given by the shape functions of finite elements [20], thus providing a natural interface to numerical simulations [11], and where mature meshing techniques allow for an arbitrarily fine fit to the sample boundaries (and potentially microstructure if wanted [12, 13]). The "best" displacement field is the argument that minimizes a functional qualifying image registration. The price to be paid for this formulation is that unknowns (i.e., nodal displacements) are coupled, unlike the local approach where each sub-volume is treated independently. Thus, parallel processing is simple

for the local approach, but requires skills used in the field of computational mechanics for global DVC [32]. Among the different variants, a very generic one is based on finite element decompositions for the displacement field, with an image-driven mesh with C8 elements (8-node cubes with trilinear displacement shape functions). However, unstructured meshes based on the imaged microstructure were also implemented in such global framework (e.g., 4-noded tetrahedra with linear displacement interpolations [12]).

The material studied below is light gypsum. Cylinders (17 mm in diameter) were extracted from industrial plasterboard plates. In situ experiments with a spherical indenter (6 mm in diameter) were performed. The specimen was imaged during unloading, and loaded at nine different levels [37]. After each step, the crosshead was held still to allow relaxation to take place for a 20-min dwell duration before acquiring a new scan. Figure 5 shows the reconstructed volumes of the sample observed by CT for the reference configuration (Fig. 5a) and the eighth load level (Fig. 5b). The compacted area is clearly visible in the upper part of the 3D rendering. It was hidden in the following DVC analyses because the gray level conservation was not satisfied. First, a C8-DVC analysis was performed for an area close to the compacted region. The corresponding longitudinal displacement field is shown in Fig. 7a for a discretization with 6-voxel long elements. Displacement fluctuations are clearly visible because the dynamic range is very small (i.e., less than 2 voxels) due to the fact that apart from the compacted volume, the plaster remained essentially elastic. Many of these fluctuations were due to measurement uncertainties associated with very small element sizes. This first analysis shows that even with very small element sizes, global DVC provided a good first estimate of the displacement field. However, it was corrupted by measurement uncertainties and the evaluation of strains cannot be carried out faithfully on such a small scale. In the next section, an alternative route will be followed.

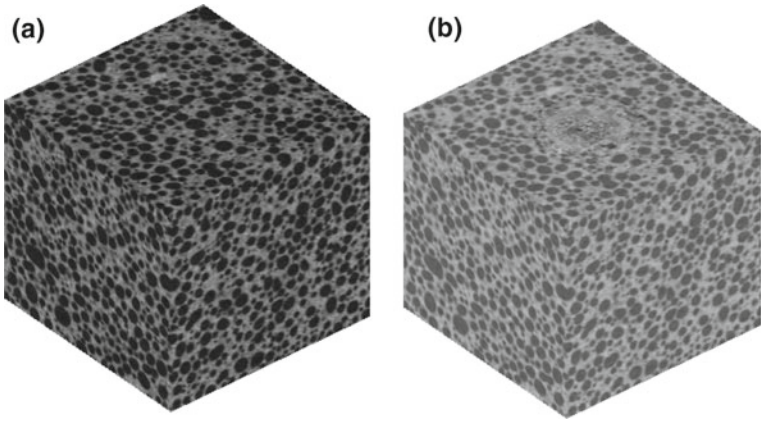

Fig. 5 3D renderings of the observed volume of interest. **a** Reference configuration, and **b** deformed configuration

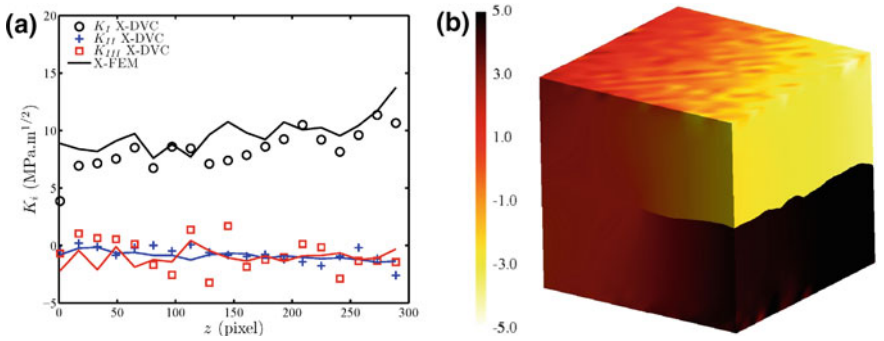

Fig. 6 **a** Profiles of K_I, K_{II} and K_{III} stress intensity factors determined experimentally by post-processing X-DVC results, and numerically via X-FEM analyses. **b** 3D rendering of the longitudinal displacement field calculated by X-FEM in the cracked nodular graphite cast iron (Fig. 1b). The scale bar is expressed in micrometers. The boundary conditions used for the calculation correspond to the experimental displacements obtained by X-DVC (after [38])

The following analysis now focuses on nodular graphite cast iron (Fig. 1b). A larger sample was first pre-cracked in fatigue. A smaller sample was cut and then tested in situ for different propagation stages [38]. After 45 kcycles, a scan was acquired at maximum and minimum load. The displacement field was first measured via C8-DVC. Using the correlation residuals (as shown in Fig. 2a), an enriched kinematics was sought using the same kinematic assumptions as in eXtended Finite Element Methods (X-FEM) [39, 40], which is called eXtended Digital Volume Correlation (or X-DVC [11, 38, 41]). The crack front was determined by projecting the displacement field measured on the Williams' series, in particular by canceling out the amplitude associated with the first supersingular field.

Another result of this procedure was the stress intensity profiles (Fig. 6a). The latter was compared with the predicted profiles having the same cracked surface, the same front and the measured boundary conditions applied to the upper and lower faces of the considered volume (Fig. 6b). A very good agreement was observed between the experimentally determined and numerically predicted stress intensity profiles. Such a result shows the interest of combining advanced experimental and numerical tools to analyze 3D cracks.

3.3 Reduced Bases and Integrated DVC

The analysis of displacements both for local and global DVC typically results from a compromise between spatial resolution and displacement uncertainty [32, 42]. To enhance the spatial resolution, smaller sub-volumes (local DVC) or elements (global DVC) are to be used to allow for local adjustments. However, this leads to an increase in the number of unknowns, and hence less available information for each

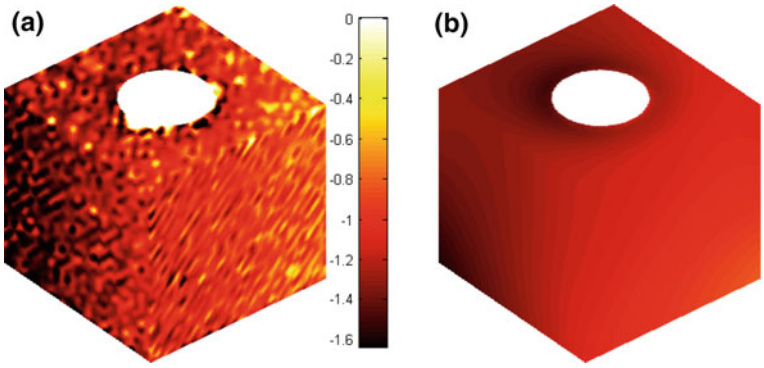

Fig. 7 3D rendering of the longitudinal displacement field measured during an indentation test on plasterboard (Fig. 1a). The zone where the material was compacted was removed. **a** Standard DVC approach. **b** DVC approach with reduced basis. The scale bar is expressed in voxels (1 voxel $\leftrightarrow$ 48 µm)

one. Consequently, the measurement uncertainty increases, so does the sensitivity to noise. This may be tolerable for displacement measurements, but soon becomes harmful to the determination of strain fields.

One possibility to circumvent this problem is to design a reduced basis, i.e., selecting much less numerous degrees of freedom, yet being faithful to the actual displacement within the specimen. The advantage of this approach is that one may easily benefit from prior knowledge on the expected displacement field. However, this knowledge cannot be expressed as analytical solutions since they are very scarce in 3D situations. Conversely, a specific basis can be built numerically as soon as the "true" unknowns of the problem are parameterized using any finite-element code [12, 43, 44].

To exemplify this concept, let us revert to the example of plasterboard indentation of the previous section. The specimen was expected to behave elastically away from the indentation. The "true" unknowns describe the loading along the boundary of the elastic domain. When a spherical harmonics decomposition of the unknown displacement on the surface of the crushed region was performed, a truncation to low order terms constituted a suited reduced basis with less than 10 degrees of freedom [43]. This displacement basis was obtained from a finite element simulation of the whole sample assumed to behave elastically. The DVC results with this reduced kinematic basis are shown in Fig. 7b. Many of the fluctuations were filtered out when compared to a standard C8-DVC result (Fig. 7a), yet the long wave features were still captured. Because the correlation residuals in both analyses were virtually identical, the DVC results with a reduced basis were deemed trustworthy.

The previous analyses can be extended to cases in which the parameters of constitutive models become the unknowns to the registration problem (as were boundary conditions in the above example). Consequently, the sought displacement fields are parameterized by these unknowns (and no longer by the nodal displacements) and can

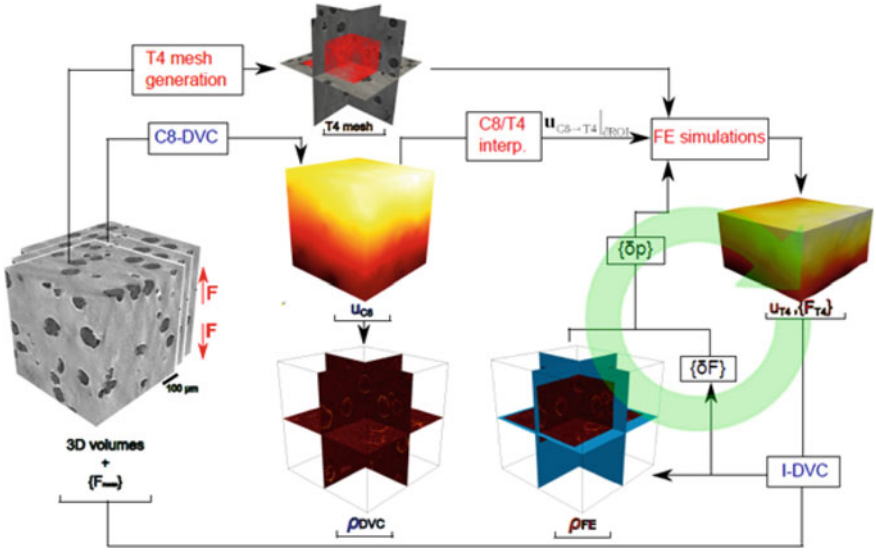

Fig. 8 Schematic representation of procedures that can be used for validation and identification purposes of numerical simulations at the microscopic scale using 3D images (adapted from [44])

be computed via finite element analyses. Such fields then satisfy equilibrium, compatibility and the selected constitutive equation. Such approaches that use mechanically admissible solutions are referred to as integrated-DVC [12]. Reduced bases are then constructed from the sensitivity fields, namely spatiotemporal displacement field derivatives with respect to the sought material parameters. Non-intrusive procedures were devised in which the 4D sensitivity fields are obtained with existing (commercial or academic) finite element codes, thereby allowing for a large versatility in meshing and incorporation of complex constitutive laws. Further, Model Order Reduction techniques like the Proper Orthogonal Decomposition [45] can be applied to these sensitivity fields [46]. Proper Generalized Decompositions (PGD [47–51]) are an alternative route that is worth investigating.

Given the fact that microtomography and laminography enable for micrometer resolutions, frameworks combining in-situ experiments and numerical simulations (Fig. 8) can be devised to validate calculations at the microscopic scale [13]. In such analyses, the region of interest in the reconstructed volume was analyzed by DVC to measure displacement fields. Finite element calculations, which took into account the details of the microstructure of cast iron (µFE [52]), were carried out using boundary conditions extracted from DVC calculations, which was a primary quantity to validate such simulations [53]. The correlation residuals of DVC *and* coupled DVC-µFE were then used for validating the measurements *and* numerical simulations. These independent results could then compared to assess the predictive capacity of the selected models [13, 53].

An identification procedure can be devised by extending the previous framework to determine (microscopic) constitutive parameters for the analysis, say, of ductile damage. It consists in the full integration of sensor (e.g., load cell) and imaging data into numerical procedures for the purpose of reducing the gray level residuals and gap between measured and computed load (Fig. 8). Such integrated approaches were performed at meso- and micro-scales [5, 12, 44]. For instance, the three mechanisms of ductile damage (i.e., nucleation, growth and coalescence) were analyzed using numerical simulations at the microscopic scale [44].

3.4 Regularized DVC

The previous strategy calls for a rather strong prior knowledge (i.e., an elastic behavior was assumed over most of the domain of the indentation test). It is also possible to introduce such information in a tunable manner allowing for a more flexible tool [32, 54, 55]. The spirit of mechanical regularization consists in adding to the traditional DVC objective functional, which is based on the quadratic difference between the deformed image corrected by a displacement field and the reference image, a second functional based on the "equilibrium gap" that penalizes deviations of the displacement field from being the solution to a homogeneous elastic problem with known (or null) body forces [56]. The latter functional is the quadratic norm of a linear second-order differential operator acting on the displacement field, and hence the relative weights given to both functionals introduce a length scale ℓ_{reg}. Below ℓ_{reg}, the regularization functional dominates, whereas at large length scales (i.e., above ℓ_{reg}), the DVC functional is the largest. This combination acts as a low-pass filter for DVC, where the high frequency component is brought by elasticity. In some sense, the previous (i.e., integrated) approach corresponds to the limit of a very large weight being given to the regularization as the library of proposed displacement fields obeys exactly elasticity over the entire domain. When a smaller value of the cut-off wavelength is used, the effect of regularization can be compared to that of a coarse mesh of size ℓ_{reg}, with however much better smoothness properties. The same method can be extended to more complex mechanical behavior than linear elasticity or heterogeneous elastic properties if desired. However, even if homogeneous linear elasticity is used, the latter can simply be considered as a smoothening operator to make the problem well-posed rather than an accurate description of the mechanical behavior of the studied specimen.

The following analysis deals with an in situ tearing test on an aluminum alloy sheet observed via synchrotron laminography. Experimental conditions for a similar material are found in Refs. [57, 58]. The present case was deemed difficult, if not impossible, since the volume fraction of secondary particles was of the order of 0.3–0.4% (Figs. 3a and 4a). Although this condition may seem impossible for DVC, the mean distance between inclusions was of the order of 7 voxels. It became even more difficult after filtering (Figs. 3b and 4b). In the unfiltered case, standard global C8-DVC (with 16-voxel elements) was performed on a zone far from the notch where

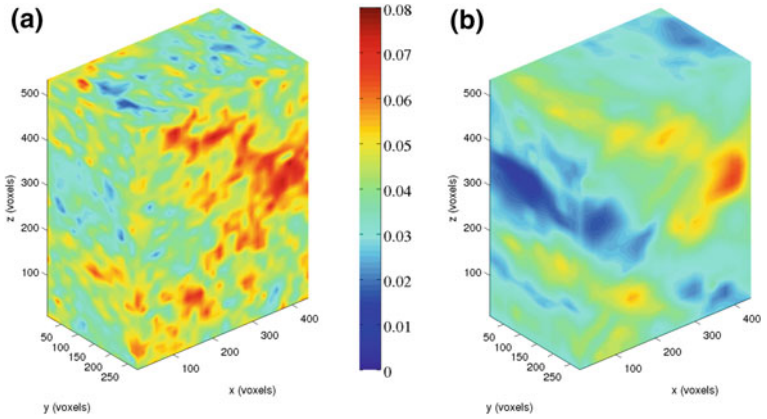

Fig. 9 3D rendering of von Mises' equivalent strain measured during an opening test of a notched aluminum alloy sample (Fig. 1c). **a** Standard DVC, and **b** regularized DVC

the crack initiated and subsequently propagated. The crack had not yet propagated even though localized bands were observed (Fig. 9a). In Fig. 9b, a regularized correlation approach (with $\ell_{reg} = 50$ voxels) is used with the same mesh as previously. However, the considered displacements were filtered. Without the present regularization, the registrations was not possible. Although the texture was extremely poor, very consistent results were observed between the equivalent strain maps obtained by both approaches (Fig. 9). The filtering of the strain field is clearly apparent, thereby illustrating its denoising effect for DVC. The question of the possible detrimental effect of this "filter" had to be evaluated on the quality of the registration, namely on the correlation residual or the difference between the reference and deformed image after correction by the measured displacement field. In that case, the quality of registration was excellent so that the filtering was not considered as detrimental to the measured displacement field.

The regularization strategy allows the DVC problem to be made well-posed even when discretized onto a very fine mesh. It was shown that the ultimate limit of a regular cubic mesh with elements reduced to a single voxel could be handled with such a strategy [54]. However, in that case, the number of unknowns becomes very large, the regularization kernel involves a more complex problem to solve, and hence regularized DVC becomes much more demanding in terms of computation time and memory management. To overcome this difficulty, a dedicated GPU implementation was set up, which could handle several million degrees of freedom within an acceptable time (i.e., less than 10 min [32]).

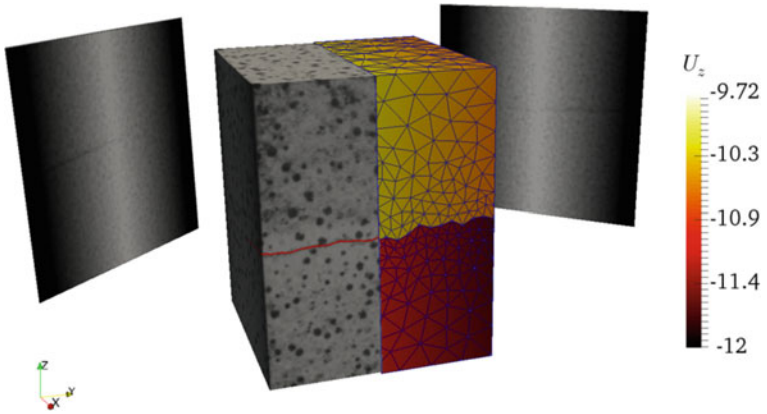

Fig. 10 Crack opening in the sample shown in the center can be obtained from an initial tomography, two projections in the deformed state and an appropriate model schematized by the finite element mesh onto which the vertical component of the displacement field is rendered and color-coded

3.5 Projection-Based DVC

When considering the temporal changes of a specimen, its microstructure usually does not change much in time but for its deformation. Hence, after a first reconstruction has been performed, the only remaining unknowns are the sample kinematics. The latter generally requires much less data than the number of voxels [59], and even more so if a mechanical model is involved [60, 61]. Performing successive reconstructions is both costly and unnecessary. It is therefore natural to try to read the kinematics directly in the radiographs, and to reduce their number (or rather increase the time resolution). This procedure, which is referred to as Projection-based DVC [59, 62], was shown to be effective with several orders of magnitude gain in needed number of projections.

Figure 10 shows the displacement field of a cracked nodular graphite cast iron sample by considering two radiographs of the deformed state. In this particular case, the unknowns were the 2×6 degrees of freedom used as boundary conditions to an elastic model in which the crack was explicitly accounted for. Further, when the reference scan is performed when the sample is unloaded (or very modestly preloaded), then the number of radiographs needed for tracking the 3D space plus time changes of the test can be reduced from 500 to 1000 down to a single one per time step [63, 64]. With this procedure, the sample was continuously loaded, continuously rotated and regularly imaged via 2D X-ray projections. Consequently, the lower spatial sampling of projection-based DVC (i.e., down to one radiograph per load level) was compensated by increasing the temporal sampling and leading to 4D analyses for which PGD turned out to be a very powerful tool to perform the projection-based registration solely over the relevant modes.

4 Conclusion

The emergence and development of full-field measurements in the bulk of imaged materials has transformed experimental solid mechanics, where huge and ever increasing amounts of data are routinely collected during tests [46]. Processing this experimental information has led to specific and elaborate numerical developments integrating measurements and simulations into unique frameworks. Integrated DVC as described herein, namely merging DVC and numerical tools traditionally used in computational mechanics (e.g., Finite Element Methods) constitutes an emblematic example. Efficient numerical GPU implementation of the resulting algorithms is also a route that can be followed.

It is expected that much more could be performed regarding time and memory savings while keeping all the relevant information (including uncertainties). Some possibly more efficient reduction techniques are related to the use of, for instance, modified POD with the metric associated with the covariance matrix for the mode selection or PGD [46]. The latter in particular will be the subject of future work as a very promising and efficient solution generator at measurement and identification stages.

In spite of the challenges listed herein, DVC was made operational and reliable for a wider class of materials than usually considered. As demonstrated herein, those extensions require a critical consideration of the reconstructed images and possibly filtering to (at least partially) erase imaging artifacts, regularization strategies to allow for noise reduction on strain evaluation and to compensate for poor microstructural contrast. Such developments are essential for fully benefiting from lab scale tomograph equipment and analyze in-situ mechanical testing to get more qualitative and quantitative insight into the mechanical behavior of materials.

Acknowledgements Different parts of the above mentioned studies were funded by Agence Nationale de la Recherche under the grants ANR-10-EQPX-37 (MATMECA) and ANR-14-CE07-0034-02 (COMINSIDE), Saint Gobain, SAFRAN Aircraft Engines and SAFRAN Tech. It is a pleasure to acknowledge the support of BPI France within the DICCIT project, and ESRF for MA1006, MI1149, MA1631, MA1932 and ME1366 experiments.
Fruitful discussions with Profs. Olivier Allix, Marc Bernacki, Pierre-Olivier Bouchard, Jean-Yves Buffière, and Drs. Jérôme Adrien, Dominique Bernard, Xavier Brajer, René Gy, Lukas Helfen, Nathalie Limodin, Eric Maire, Thilo Morgeneyer, Estelle Parra, Julien Réthoré and Julien Schneider are acknowledged.

References

1. Bay, B. K. (2008). Methods and applications of digital volume correlation. *Journal Strain Analysis*, *43*, 745.
2. Helfen, L., Baumbach, T., Mikulik, P., Kiel, D., Pernot, P., Cloetens, P., et al. (2005). High-resolution three-dimensional imaging of flat objects by synchrotron-radiation computed laminography. *Applied Physics Letters*, *86*(7), 071915.

3. Sutton, M. A., Orteu, J. J., & Schreier, H. (2009). *Image correlation for shape, motion and deformation measurements: Basic concepts, theory and applications*. New York, NY (USA): Springer.
4. Hild, F., & Roux, S. (2012). Digital image correlation. In P. Rastogi & E. Hack (Eds.), *Optical methods for solid mechanics. A full-field approach* (pp. 183–228). Weinheim (Germany): Wiley-VCH.
5. Buljac, A., Jailin, C., Mendoza, A., Taillandier-Thomas, T., Bouterf, A., Neggers, J., et al. (2018). Digital volume correlation: Review on progress and challenges. *Experimental Mechanics, 58*(5), 661–708.
6. Baruchel, J., Buffière, J. Y., Maire, E., Merle, P., & Peix, G. (Eds.). (2000). *X-Ray tomography in material sciences*. Paris (France): Hermès Science.
7. Weitkamp, T., Tafforeau, P., Boller, E., Cloetens, P., Valade, J., Bernard, P., et al. (2010). Status and evolution of the ESRF beamline ID19. In *ICXOM 2009* (AIP Conference Proceedings) (Vol. 1221, pp. 33–38)
8. Maire, E., & Withers, P. J. (2014). Quantitative X-ray tomography. *International Materials Reviews*, *59*(1), 1–43.
9. Wikipedia Contributors. (2019). Industrial computed tomography. *Wikipedia, The Free Encyclopedia* p. 883448937.
10. Buffière, J. Y., Maire, E., Adrien, J., Masse, J. P, & Boller, E. (2010). In Situ Experiments with X ray Tomography: An Attractive Tool for Experimental Mechanics. *Experimental Mechanics*, *50*(3), 289–305.
11. Rannou, J., Limodin, N., Réthoré, J., Gravouil, A., Ludwig, W., Baïetto, M., et al. (2010). Three dimensional experimental and numerical multiscale analysis of a fatigue crack. *Computer Methods in Applied Mechanics and Engineering*, *199*, 1307–1325.
12. Hild, F., Bouterf, A., Chamoin, L., Mathieu, F., Neggers, J., Pled, F., et al. (2016). Toward 4D mechanical correlation. *Advanced Modeling and Simulation in Engineering Sciences*, *3*(1), 1–26.
13. Buljac, A., Shakoor, M., Bernacki, M., Bouchard, P. O., Morgeneyer, T. F., & Hild, F. (2017). Numerical validation framework for micromechanical simulations based on synchrotron 3D imaging. *Computational Mechanics*, *59*(3), 419–441.
14. Bornert, M., Chaix, J. M., Doumalin, P., Dupré, J. C., Fournel, T., Jeulin, D., et al. (2004). Mesure tridimensionnelle de champs cinématiques par imagerie volumique pour l'analyse des matériaux et des structures. *Institute Mes Métrology*, *4*, 43–88.
15. Ludwig, W., Buffière, J. Y., Savelli, S., & Cloetens, P. (2003). Study of the interaction of a short fatigue crack with grain boundaries in a cast Al alloy using X-ray microtomography. *Acta Materials*, *51*(3), 585–598.
16. Buffière, J. Y., Maire, E., Cloetens, P., Lormand, G., & Fougères, R. (1999). Characterisation of internal damage in a MMCp using X-ray synchrotron phase contrast microtomography. *Acta Materials*, *47*(5), 1613–1625.
17. Helfen, L., Baumbach, T., Cloetens, P., & Baruchel, J. (2009). Phase contrast and holographic computed laminography. *Applied Physics Letters*, *94*, 104103.
18. Altapova, V., Helfen, L., Myagotin, A., Hänschke, D., Moosmann, J., Gunneweg, J., et al. (2012). Phase contrast laminography based on talbot interferometry. *Optics Express*, *20*, 6496–6508.
19. Bay, B. K., Smith, T. S., Fyhrie, D. P., & Saad, M. (1999). Digital volume correlation: Three-dimensional strain mapping using X-ray tomography. *Experimental Mechanics*, *39*, 217–226.
20. Roux, S., Hild, F., Viot, P., & Bernard, D. (2008). Three dimensional image correlation from X-Ray computed tomography of solid foam. *Composites Part A*, *39*(8), 1253–1265.
21. Hall, S., Bornert, M., Desrues, J., Pannier, Y., Lenoir, N., Viggiani, C., et al. (2010). Discrete and continuum analysis of localized deformation in sand using X-ray micro CT and volumetric digital image correlation. *Géotechnique*, *60*(5), 315–322.
22. Hild, F., Fanget, A., Adrien, J., Maire, E., & Roux, S. (2011). Three dimensional analysis of a tensile test on a propellant with digital volume correlation. *Archives of Mechanics*, *63*(5–6), 1–20.

23. Limodin, N., Réthoré, J., Adrien, J., Buffière, J. Y., Hild, F., & Roux, S. (2011). Analysis and artifact correction for volume correlation measurements using tomographic images from a laboratory X-ray source. *Experimental Mechanics*, *51*(6), 959–970.
24. Vidal, F. P., Letang, J. M., Peix, G., & Cloetens, P. (2005). Investigation of artifact sources in synchrotron microtomography via virtual X-ray imaging. *Nuclear Instruments and Methods in Physics Research*, *234*, 333–348.
25. Prell, D., Kyriakou, Y., & Kalender, W. A. (2009). Comparison of ring artifact correction methods for flat-detector CT. *Physics in Medicine and Biology*, *54*, 3881–3895.
26. Jailin, C., Buljac, A., Bouterf, A., Poncelet, M., Hild, F., & Roux, S. (2018). Self-calibration for lab-mct using space-time regularized projection-based dvc and model reduction. *Measurement Science and Technology*, *29*, 024003.
27. Dahdah, N., Limodin, N., El Bartali, A., Witz, J. -F., Seghir, R., Charkaluk, E., et al. (2016). Damage investigation in A319 aluminium alloy by X-ray tomography and digital volume correlation during in situ high-temperature fatigue tests. *Strain*, *52*(4), 324–335.
28. Cai, B., Karagadde, S., Yuan, L., Marrow, T. J., Connolley, T., & Lee, P. D. (2014). In situ synchrotron tomographic quantification of granular and intragranular deformation during semi-solid compression of an equiaxed dendritic Al-Cu alloy. *Acta Materials*, *76*, 371–380.
29. Maire, E., Le Bourlot, C., Adrien, J., Mortensen, A., & Mokso, R. (2016). 20-Hz X-ray tomography during an in situ tensile test. *International Journal of Fracture*, *200*(1), 3–12.
30. Feldkamp, L. A., Davis, L. C., & Kress, J. W. (1984). Practical cone beam algorithm. *The Journal of the Optical Society of America*, *1*, 612–619.
31. Gabor, G. T. (2009). *Fundamentals of computerized tomography: Image reconstruction from projections*. London (UK): Springer.
32. Leclerc, H., Périé, J. N., Hild, F., & Roux, S. (2012). Digital volume correlation: What are the limits to the spatial resolution? *Mechanical and Industrial*, *13*, 361–371.
33. Herman, G. T., & Davidi, R. (2008). Image reconstruction from a small number of projections. *Inverse Problems*, *24*, 045011.
34. Hild, F., & Roux, S. (2012). Comparison of local and global approaches to digital image correlation. *Search Results*, *52*(9), 1503–1519.
35. Sutton, M. A. (2013). Computer vision-based, noncontacting deformation measurements in mechanics: A generational transformation. *Applied Mechanics Reviews, 65* (AMR-13-1009), 050802.
36. Smith, T. S., Bay, B. K., & Rashid, M. M. (2002). Digital volume correlation including rotational degrees of freedom during minimization. *Experimental Mechanics*, *42*(3), 272–278.
37. Bouterf, A., Adrien, J., Maire, E., Brajer, X., Hild, F., & Roux, S. (2017). Identification of the crushing behavior of brittle foam: From indentation to oedometric tests. *Journal of the Mechanics and Physics of Solids*, *98*, 181–200.
38. Réthoré, J., Limodin, N., Buffière, J. Y., Hild, F., Ludwig, W., & Roux, S. (2011). Digital volume correlation analyses of synchrotron tomographic images. *The Journal of Strain Analysis*, *46*, 683–695.
39. Black, T., & Belytschko, T. (1999). Elastic crack growth in finite elements with minimal remeshing. *The International Journal for Numerical Methods in Engineering*, *45*, 601–620.
40. Moës, N., Dolbow, J., & Belytschko, T. (1999). A finite element method for crack growth without remeshing. *The International Journal for Numerical Methods in Engineering*, *46*(1), 133–150.
41. Réthoré, J., Tinnes, J. P., Roux, S., Buffière, J., & Hild, F. (2008). Extended three-dimensional digital image correlation. textitComptes Rendus Mécanique, *336*, 643–649.
42. Buljac, A., Taillandier-Thomas, T., Helfen, L., Morgeneyer, T., & Hild, F. (2018). Evaluation of measurement uncertainties of digital volume correlation applied to laminography data. *The Journal of Strain Analysis*, *53*, 49–65.
43. Bouterf, A., Roux, S., Hild, F., Adrien, J., & Maire, E. (2014). Digital volume correlation applied to X-ray tomography images from spherical indentation tests on lightweight gypsum. *Strain*, *50*(5), 444–453.

44. Buljac, A., Trejo-Navas, V. -M., Shakoor, M., Bouterf, A., Neggers, J., Bernacki, M., et al. (2018). On the calibration of elastoplastic parameters at the microscale via X-ray microtomography and digital volume correlation for the simulation of ductile damage. *European Journal of Mechanics*, *72*, 287–297.
45. Chatterjee, A. (2000). An introduction to the proper orthogonal decomposition. *Current Science*, *78*(7), 808–817.
46. Neggers, J., Allix, O., Hild, F., & Roux, S. (2018). Big data in experimental mechanics and model order reduction: Today's challenges and tomorrow's opportunities. *Archives of Computational Methods in Engineering*, *25*(1), 143–164.
47. Chinesta, F., Ammar, A., & Cueto, E. (2010). Recent advances and new challenges in the use of the proper generalized decomposition for solving multidimensional models. *Archives of Computational Methods in Engineering*, *17*(4), 327–350.
48. Ladevèze, P., Passieux, J. -C., & Néron, D. (2010). The LATIN multiscale computational method and the proper generalized decomposition. *Computer Methods in Applied Mechanics and Engineering*, *199*(21), 1287–1296.
49. Nouy, A. (2010). Proper generalized decompositions and separated representations for the numerical solution of high dimensional stochastic problems. *Archives of Computational Methods in Engineering*, *17*(4), 403–434.
50. Ladevèze, P. (2014). PGD in linear and nonlinear computational solid mechanics. In *Separated representations and PGD-based model reduction* (pp. 91–152). Berlin: Springer.
51. Paillet, C., Néron, D., & Ladevèze, P. (2018). A door to model reduction in high-dimensional parameter space. *Comptes Rendus Mécanique*, *346*(7), 524–531.
52. Shakoor, M., Bouchard, P. O., & Bernacki, M. (2017). An adaptive level-set method with enhanced volume conservation for simulations in multiphase domains. *The International Journal for Numerical Methods in Engineering*, *109*(4), 555–576.
53. Shakoor, M., Buljac, A., Neggers, J., Hild, F., Morgeneyer, T. F., Helfen, L., et al. (2017). On the choice of boundary conditions for micromechanical simulations based on 3D imaging. *International Journal of Solids and Structures*, *112*, 83–96.
54. Leclerc, H., Périé, J. N., Roux, S., & Hild, F. (2011). Voxel-scale digital volume correlation. *Experimental Mechanics*, *51*(4), 479–490.
55. Taillandier-Thomas, T., Roux, S., Morgeneyer, T. F., & Hild, F. (2014). Localized strain field measurement on laminography data with mechanical regularization. *Nuclear Instruments and Methods in Physics Research*, *324*, 70–79.
56. Claire, D., Hild, F., & Roux, S. (2002). Identification of damage fields using kinematic measurements. *Comptes Rendus Mécanique*, *330*, 729–734.
57. Morgeneyer, T. F., Helfen, L., Sinclair, I., Proudhon, H., Xu, F., & Baumbach, T. (2011). Ductile crack initiation and propagation assessed via in situ synchrotron radiation computed laminography. *Scripta Materialia*, *65*, 1010–1013.
58. Morgeneyer, T. F., Helfen, L., Mubarak, H., & Hild, F. (2013). 3D digital volume correlation of synchrotron radiation laminography images of ductile crack initiation: An initial feasibility study. *Experimental Mechanics*, *53*(4), 543–556.
59. Leclerc, H., Roux, S., & Hild, F. (2015). Projection savings in CT-based digital volume correlation. *Experimental Mechanics*, *55*(1), 275–287.
60. Taillandier-Thomas, T., Roux, S., & Hild, F. (2016). Soft route to 4D tomography. *Physical Review Letters*, *117*(2), 025501.
61. Taillandier-Thomas, T., Jailin, C., Roux, S., Hild, F. (2016). Measurement of 3D displacement fields from few tomographic projections. In *Proceedings of SPIE, Optics, Photonics and Digital Technologies for Imaging Applications IV* (Vol. 9896L, p. 98960L).
62. Khalili, M. H., Brisard, S., Bornert, M., Aimedieu, P., Pereira, J. M., & Roux, J. N. (2017). Discrete digital projections correlation: A reconstruction-free method to quantify local kinematics in granular media by X-ray tomography. *Experimental Mechanics*, *57*(6), 819–830.

63. Jailin, C., Buljac, A., Bouterf, A., Hild, F., & Roux, S. (2018). Fast 4D tensile test monitored via X-CT: Single projection based digital volume correlation dedicated to slender samples. *Journal of Strain Analysis*, *53*(7), 473–484.
64. Jailin, C., Buljac, A., Bouterf, A., Hild, F., & Roux, S. (2019). Fast four-dimensional tensile test monitored via X-ray computed tomography: Elastoplastic identification from radiographs. *Journal of Strain Analysis*, *54*(1), 44–53.

Manufacturing and Virtual Design to Tailor the Properties of Boron-Alloyed Steel Tubes

Illia Hordych, Sebastian Herbst, Florian Nürnberger, Viacheslav Boiarkin, Olivier Hubert and Hans Jürgen Maier

Abstract Application of products with properties locally adapted for specific loads and requirements has become widespread in recent decades. In the present study, an innovative approach to manufacture tubes with tailored properties in the longitudinal direction from a boron-alloyed steel 22MnB5 was developed. Due to advanced heating and cooling strategies, a wide spectrum of possible steel phase compositions can be obtained in tubes manufactured in a conventional tube forming line. A heat-treatment station placed after the forming line is composed of an inductive heating and an adapted water-air cooling spray system. These short-action processes allow fast austenitizing and subsequent austenite decomposition within several seconds. To describe the effect of high inductive heating rates on austenite formation, dilatometric investigations were performed in a heating rate range from 500 to 2500 K s^{-1}. A completed austenitizing was observed for the whole range of the investigated heating rates. The austenitizing was described using Johnson-Mehl-Avrami model. Furthermore, series of experiments on heating and cooling with different cooling rates in the developed technology line was carried out. Complex microstructures were obtained for the cooling in still as well as with compressed air, while the water-air cooling at different pressures resulted in quenched martensitic microstructures. Nondestructive testing of the mechanical properties and the phase composition was realized by means of magnetization measurements. Logarithmic models to predict the phase composition and hardness values from the magnetic properties were obtained. Subsequently, a simulation model allowing virtual design of tubes in the FE-software ANSYS was developed on basis of experimental data. The model is suited to predict microstructural and mechanical properties under consideration of the actual process parameters.

I. Hordych (✉) · S. Herbst · F. Nürnberger · H. J. Maier
Institut für Werkstoffkunde (Materials Science), Leibniz Universität Hannover, Hannover, Germany
e-mail: hordych@iw.uni-hannover.de

V. Boiarkin
Department of Metal Forming, National Metallurgical Academy of Ukraine, Dnipro, Ukraine

O. Hubert
Laboratoire de Mécanique et Technologie, Ecole Normale Supérieure Paris Saclay, Cachan, France

P. Wriggers et al. (eds.), *Virtual Design and Validation*, Lecture Notes in Applied and Computational Mechanics 93, https://doi.org/10.1007/978-3-030-38156-1_2

1 Introduction

In the pursuit of economic and ecologic manufacturing processes, different products that can be adapted to local loadings and stresses have been developed. From this point of view, tailored components are attractive due to the possibility of their local adjustment to application purposes. Different technological strategies can be employed in order to tailor the mechanical properties of products [1], which can be divided into two main groups: in the first one, tailoring is achieved by combining materials with different properties. In this case, dissimilar materials are combined through the creation of metallurgical, form- or force-closed joints depending on their unique characteristics [2, 3]. The second group assembles methods of tailoring properties within the same material through the adaptation of geometry dimensions (e.g. rolling with alternating roll diameters) and/or microstructures (e.g. selective heat-treatment) [4]. A break-through in the industry of, above all, automotive steels that came with introduction of complex microstructures (dual-, complex-phase, TRIP-, TWIP-steels) attracted strong attention to advanced heat-treatments and the possibility of steel tailoring through miscellaneous time-temperature courses [5, 6]. In this respect, boron and manganese alloyed steels are characterized by their enhanced hardenability and a wide spectrum of possible phase compositions achievable by heat-treatments. In addition, they exhibit a high level of mechanical and wear properties in service [7].

The present investigation aims to develop and implement a technology line, which allows the manufacturing of tailored tubes based on locally adapted mechanical properties in the longitudinal direction by means of an advanced heat-treatment integrated in the production line. Being a continuous process, tube forming is advantageous for integration of a local heat-treatment station to manufacture hollow profiles with a constant cross-section over the length. When using boron-alloyed steels, a significant delay of ferrite-perlite formation during the cooling due to the boron addition technologically simplifies an achievement of different steel phases. Depending on the cooling rate, diffusive (ferrite-perlite, bainite) as well as diffusionless (martensite) transformations can take place [8]. This implies that by a selective heat-treatment and adapted heating/cooling strategies, different combinations of phase compositions can be obtained, such as relatively ductile ferrite-perlitic or bainitic and hard martensitic sections. Such tailored tubes can:

- Be post processed as semi-finished products: for the manufacturing of, e.g. T-shape tubes by means of hydroforming, certain sections to be processed can be held purposely ductile, while not affected sections will gain the final properties during the integrated heat-treatment.
- Find a direct application: for instance, ductile sections of frame rails in the automotive body can absorb the kinetic energy during a crash accident and hence, ensure a controlled deformation through a predictable folding, whereas hard sections remain responsible for the crash resistance. In addition, a damping effect of ductile sections can enhance vibration resistance of these products.